Title

Physico-electrochemical Characterization of Pluripotent Stem Cells during Self-Renewal or Differentiation by a Multi-modal Monitoring System.

Journal

Stem cell reports, 8(5)

ISSN

2213-6711

Authors

Low, Karen
Wong, Lauren Y
Maldonado, Maricela
et al.

Publication Date

2017-05-01

DOI

10.1016/j.stemcr.2017.03.021

Peer reviewed

Stem Cell Reports
Article

OPEN ACCESS

Physico-electrochemical Characterization of Pluripotent Stem Cells during Self-Renewal or Differentiation by a Multi-modal Monitoring System

Karen Low,[1,3] Lauren Y. Wong,[1,3] Maricela Maldonado,[1] Chetas Manjunath,[1] Christopher B. Horner,[1] Mark Perez,[1] Nosang V. Myung,[2] and Jin Nam[1,*]

[1]Department of Bioengineering, University of California-Riverside, Materials Science & Engineering Building 331
[2]Department of Chemical and Environmental Engineering, University of California-Riverside, Bourns Hall B355
900 University Avenue, Riverside, CA 92521, USA
[3]Co-first author
*Correspondence: jnam@engr.ucr.edu
http://dx.doi.org/10.1016/j.stemcr.2017.03.021

SUMMARY

Monitoring pluripotent stem cell behaviors (self-renewal and differentiation to specific lineages/phenotypes) is critical for a fundamental understanding of stem cell biology and their translational applications. In this study, a multi-modal stem cell monitoring system was developed to quantitatively characterize physico-electrochemical changes of the cells in real time, in relation to cellular activities during self-renewal or lineage-specific differentiation, in a non-destructive, label-free manner. The system was validated by measuring physical (mass) and electrochemical (impedance) changes in human induced pluripotent stem cells undergoing self-renewal, or subjected to mesendodermal or ectodermal differentiation, and correlating them to morphological (size, shape) and biochemical changes (gene/protein expression). An equivalent circuit model was used to further dissect the electrochemical (resistive and capacitive) contributions of distinctive cellular features. Overall, the combination of the physico-electrochemical measurements and electrical circuit modeling collectively offers a means to longitudinally quantify the states of stem cell self-renewal and differentiation.

INTRODUCTION

Human induced pluripotent stem cells (IPSCs), derived from individual patients, provide an excellent cell source for personalized regenerative medicine (Amabile and Meissner, 2009). The efficacy of IPSCs has been well documented in animal models and the first human clinical trial using patient-derived IPSCs for retinal transplant is currently ongoing (Cyranoski, 2014). In addition to their clinical applications, IPSCs also provide an ideal platform to develop patient-oriented and disease-specific in vitro models that can be utilized to understand pathological and molecular mechanisms during disease progression. For example, IPSCs have been used to study the pathology of amyotrophic lateral sclerosis by reprogramming the patient's fibroblasts to IPSCs and differentiating the cells into functional motor neurons (Burkhardt et al., 2013; Chen et al., 2014b; Egawa et al., 2012). Such IPSC-derived in vitro models are especially valuable for drug screening aimed at developing personalized pharmaceutical therapies (Ebert et al., 2012; Kim, 2014). Therefore, it is critical to quantitatively monitor the cellular behaviors during the course of IPSC self-renewal or differentiation toward specific lineages to fully utilize these diverse potentials of IPSCs.

Traditionally, stem cells have been characterized by biochemical techniques, such as PCR and immunoblotting, to determine changes in gene and protein expression. Although these traditional techniques offer semi-quantitative measurements for cellular behaviors, they are destructive in nature, which prevents tracking of specific populations of the cells throughout their biological processes. The most common non-destructive analytical method is flow cytometry, but this technique requires labeling of surface-expressed biomarker as well as detachment of the cells from substrates, thus limiting longitudinal monitoring of the cells. In this regard, physical changes of the cells, i.e., mass and morphology, provide another means to assess cellular behaviors. Stem cell proliferation or self-renewal is distinguished by increased cell quantity, which corresponds to mass change. On the other hand, differentiation is typically associated with changes in cell morphology which can be qualitatively characterized by size, shape, and structural features (Hu et al., 2010; Oldershaw et al., 2010; Wang et al., 2015). For this reason, albeit semi-quantitative at best, morphology characterization via optical microscopy has been the gold standard to routinely observe cellular behaviors.

Such physical changes in cells, occurring during self-renewal or differentiation, result in corresponding alterations in their electrical properties as the cell acts as both a resistor and a capacitor (Chen et al., 2014a; Morgan et al., 2007; Qiao et al., 2012; Venkatanarayanan et al., 2013). Diverse morphological features (i.e., cell spread, roundness, and compactness), as well as changes in the type and quantity of cell-cell and cell-substrate junctions, affect the resistive and capacitive properties of the cell layer. Electrochemical impedance spectroscopy (EIS) is an analytical method to measure such electrical properties (Randviir and Banks, 2013). This technique applies alternating current (AC) voltage perturbation at a

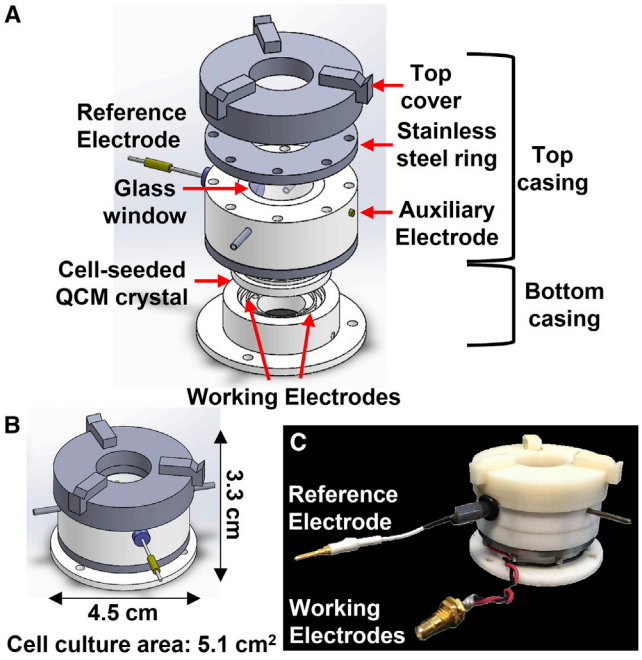

Figure 1. A Schematic of the Multi-modal QCM-EIS Device

(A) An assembly view of the device labeled for individual components.

(B) An assembled view of the device.

(C) A photograph of the prototype QCM-EIS device.

low amplitude over a range of frequencies to an electrochemical system, for example, composed of extracellular matrix, cells, and cell culture medium. Cell adhesion and its morphological changes on a substrate surface causes alterations in the impedance derived from the resistive and capacitive components of the system. Especially, spectroscopic analysis of AC impedance over a range of frequencies provides important information regarding cell-substrate and cell-cell interactions.

The electrical properties of cells were recently analyzed by EIS during the differentiation of stem cells (Angstmann et al., 2011; Bagnaninchi and Drummond, 2011; Venkatanarayanan et al., 2013). These pioneering works have demonstrated a possibility of using changes in impedance as a biomarker for stem cell behaviors. However, the studies were limited to qualitative analyses, unable to fully realize the quantitative potentials of EIS to correlate the physical (cell quantity and morphology) and electrical (resistive and capacitive) properties of the cells with stem cell self-renewal/differentiation.

In this study, we developed a cell culture system to quantitatively monitor stem cell behaviors in real time during self-renewal and differentiation of IPSCs. The system combines quartz crystal microbalance (QCM) to monitor mass changes and EIS to measure impedance, in addition to optical clearance for cell visualization. The non-destructive, label-free nature of the system allows for longitudinal monitoring of the same population of the cells. Using this QCM-EIS real-time monitoring system, mass and impedance changes of IPSCs were correlated to changes in cell quantity and morphology. Furthermore, an equivalent circuit model was utilized to further dissect the changes in resistive and capacitive electrical properties of the cells, which were correlated to the progression of IPSC self-renewal and differentiation.

RESULTS

Development of the Multi-modal Cell Monitoring System

To non-destructively and quantitatively monitor stem cell behaviors in real time, a QCM-EIS device was developed using a three-electrode setup (Figure 1). The setup incorporates the working, reference, and auxiliary electrodes used for both QCM and EIS. A polytetrafluoroethylene bottom casing houses two gold electrodes, which are in contact with the electrode pattern on the QCM crystal. The working electrodes deliver an AC potential perturbation to resonate the crystal at its resonant frequency for monitoring mass changes. An indium tin oxide (ITO) QCM crystal was used due to its transparency, which allows for visual observation of the cells during culture. The electrode on the top surface of the QCM crystal was alternatively used as the voltage source when the device was used in the EIS mode. The top casing holds the Ag/AgCl reference electrode and platinum wire auxiliary electrode to complete the three-electrode setup for the EIS system. A glass window is secured by a stainless steel ring above the top casing to provide an optical pathway while maintaining sterility during cell culture.

Morphological Characterization of IPSCs during Self-renewal and Mesendodermal/Ectodermal Differentiation

To obtain baseline morphological characteristics of IPSCs during self-renewal and differentiation, cells were cultured on Geltrex-coated tissue culture plates and subjected to either self-renewal or differentiation conditions for various durations (Figure 2). The maintenance of pluripotency in the self-renewal condition and the differentiation efficiency toward mesendodermal and ectodermal lineages under the differentiation conditions were determined by immunofluorescence imaging (Figures 2A and S1). As expected, NANOG, a marker for pluripotency, was expressed throughout the duration of the culture for the self-renewal condition. GSC expression under the mesendodermal differentiation condition gradually increased beginning at

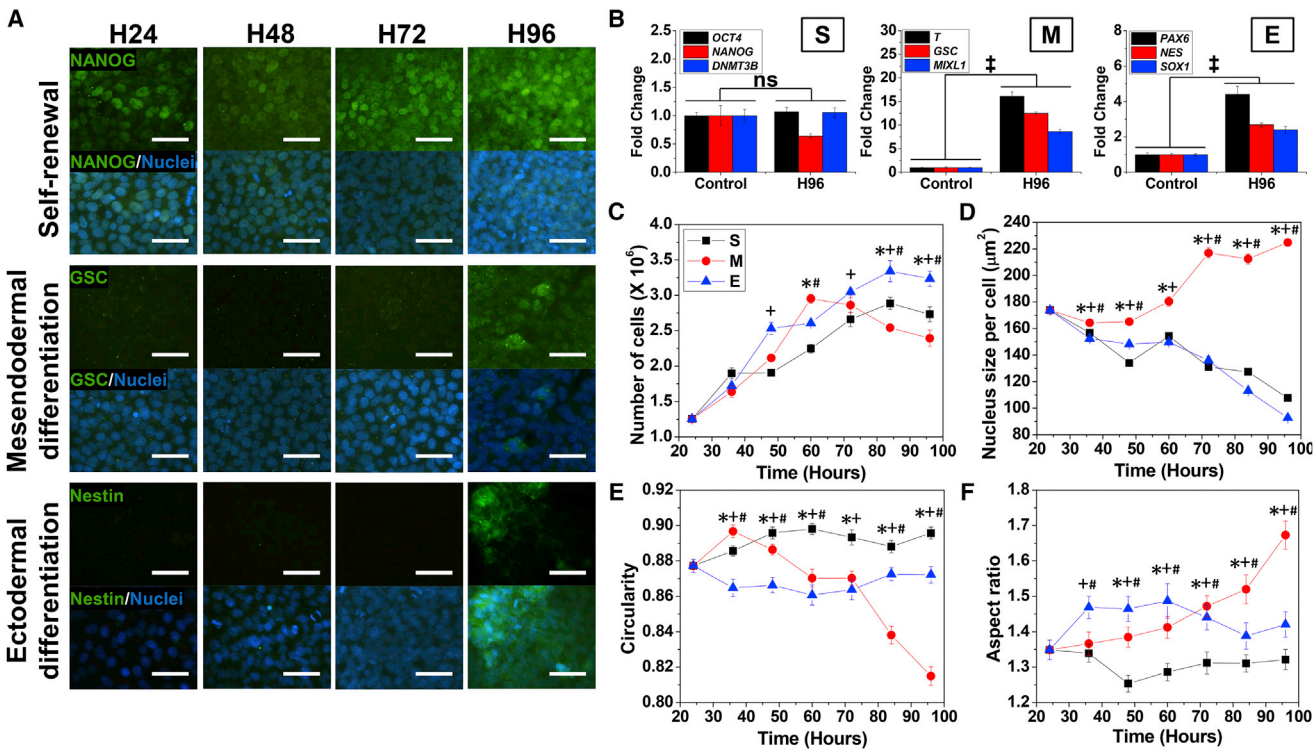

Figure 2. Characterization of Human IPSCs under Self-renewal/Differentiation Conditions and Immunofluorescence Analyses of Cell Number and Morphology

(A) Representative immunofluorescence images showing protein expression of pluripotency marker, NANOG, mesendodermal marker, GSC, and ectodermal marker, Nestin, for self-renewal, mesendodermal, and ectodermal differentiation conditions, respectively over 96 hr (blue, nucleus; green, protein of interest). Scale bar, 50 μm (see also Figure S1).

(B) Real-time PCR analysis of pluripotency (*OCT4, NANOG,* and *DNMT3B*) and differentiation (mesendodermal, *T, GSC*, and *MIXL1*; ectodermal, *PAX6, NES,* and *SOX1*) markers after 96 hr of culture (S, self-renewal; M, mesendodermal differentiation; E, ectodermal differentiation). Data are represented as mean ± SEM (n = 6; 3 biologically independent samples with technical duplicate per condition). ‡$p < 0.01$; ns, not significant.

(C–F) Comparison of (C) cell number change and cell morphology characterization, (D) nuclei coverage area, (E) circularity, and (F) aspect ratio via nuclei analysis during IPSC self-renewal and differentiation from immunofluorescence images. Data are represented as mean ± SEM (n = 450 cells from 9 different areas of three biologically independent samples). $^{*,+,\#}p < 0.05$ between S and M, S and E, and M and E, respectively.

hour 72, while Nestin, an early ectodermal marker, was detected at hour 96 for the cells subjected to the ectodermal differentiation condition.

To further confirm the pluripotency or differentiation state, gene expression after 96 hr for each condition was determined by real-time PCR (Figure 2B). For the self-renewal condition, there was no significant changes in the expression of *OCT4, NANOG,* and *DNMT3B* after 96 hr of culture in the system. For the mesendodermal differentiation condition, a significant upregulation of *T, GSC,* and *MIXL1* was observed after 96 hr. Similarly, a significant upregulation of *PAX6*, *NES*, and *SOX1* was induced by the ectodermal differentiation condition. The data, together with the protein expression analyses, indicate that the conditions utilized in this study resulted in the maintenance of the pluripotency or differentiation toward mesendodermal and ectodermal lineages.

The immunofluorescent images were utilized to determine the number of cells (Figure 2C) and cell morphology (Figures 2D–2F). Up to hour 60, all three conditions exhibited an increase in cell number. Following hour 60, self-renewal and ectodermal differentiation continued to increase in cell number, while mesendodermal differentiation began to decrease. A slight decrease in cell number was observed for all three conditions after hour 84, likely due to contact inhibition when reaching 100% confluency. The changes in cell morphology were characterized by the morphological features of individual nucleus at various time points, based on the previous reports showing a strong correlation between cell and nuclei shape (Figures

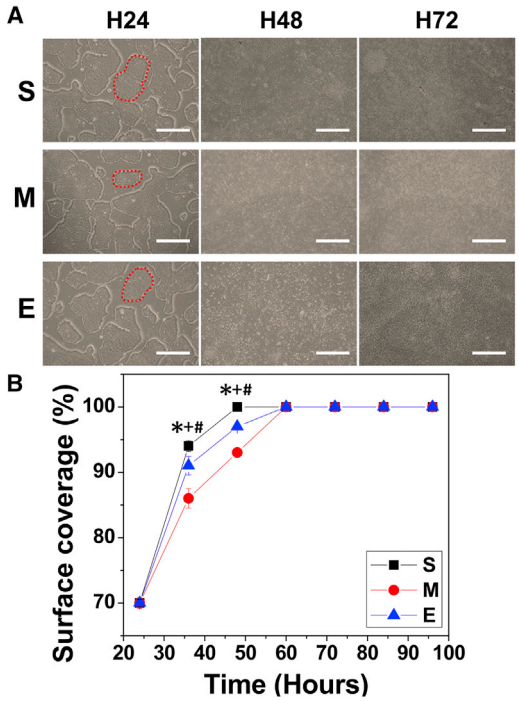

Figure 3. Optical Monitoring of IPSCs during Self-renewal or Differentiation in the QCM-EIS Device

(A) Representative optical images taken every 24 hr during the course of cell culture up to 100% confluency (see also Figure S2). Red dotted outlines represent a single cell colony within the culture. Scale bar, 1 mm.

(B) Cell surface coverage during IPSC culture quantified from optical images (S, self-renewal; M, mesendodermal differentiation; E, ectodermal differentiation). Data are represented by mean ± SEM (n = 9; 3 biologically independent samples with images from three different areas per sample). $^{*,+,\#}p < 0.05$ between S and M, S and E, and M and E, respectively.

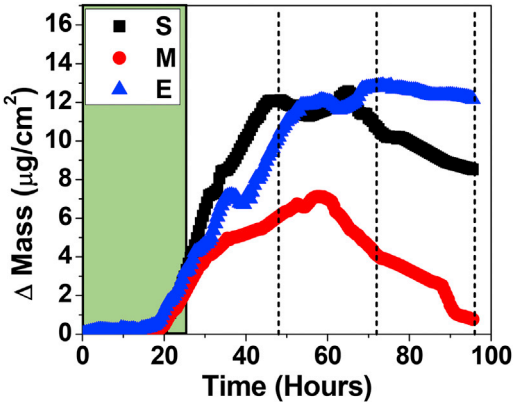

Figure 4. Mass Changes during IPSC Self-renewal or Differentiation by QCM

Representative datasets of cell mass change measured by QCM during IPSC culture. The shaded region indicates the initial self-renewal phase for all three conditions. Differentiation was induced at hour 24 for either mesendodermal or ectodermal lineage. The broken lines indicate time points used for EIS analysis at hours 48, 72, and 96 (S, self-renewal; M, mesendodermal differentiation; E, ectodermal differentiation).

2D–2F) (Versaevel et al., 2012; Vishavkarma et al., 2014). Cell size estimated from nucleus size, circularity, and aspect ratio were quantified based on their distinctive morphological changes during IPSC self-renewal and differentiation. Self-renewing cells exhibited a decrease in cell size while maintaining relatively constant values for circularity and aspect ratio. This behavior is one of the characteristics of IPSCs during self-renewal in which compact cell colonies are formed and expand (Meissner et al., 2007; Yu et al., 2007). Similarly, cells undergoing ectodermal differentiation also showed a decrease in cell size during differentiation, but they exhibited a deviation from the round cell morphology observed in the self-renewal condition. Unlike self-renewal or ectodermal differentiation, cells undergoing mesendodermal differentiation exhibited a sharp increase in cell size and aspect ratio at hour 60 and a decrease in circularity, signifying that the cells were spreading and elongating during the differentiation period.

Cell Behavior Monitoring Using a QCM-EIS Device

In comparison with imaging analysis of IPSCs cultured on tissue culture plates for various durations as described above, cells were alternatively cultured in the QCM-EIS device and subjected to the same self-renewal and differentiation conditions. Cell colony expansion was optically monitored during culture, enabled by the transparent ITO QCM crystal (Figure 3). The optical observation was conducted every 12 hr starting at hour 24 post-device assembly, which typically showed approximately 70% confluency (Figures 3A and S2). Cell coverage on the crystal was quantified from the optical images (Figure 3B). By hour 60 post-assembly, the cells for all conditions reached 100% confluency.

The optical observations in cell growth were compared with the mass changes that were continuously measured by QCM (Figure 4). During the initial 24 hr, the mass change exhibited two phases, the initial lag phase followed by a sharp increase, which is typical for the growth behavior of adherent cells. Differentiation initiated at hour 24 resulted in different mass change behaviors among the three conditions. Self-renewal and ectodermal differentiation conditions exhibited similar mass change trends up to approximately hour 48, while the mesendodermal differentiation condition showed a slower mass increase (Figure 4). After the cells reached 100% confluency at hour 60 with peak masses for all three conditions, they exhibited dramatically different behaviors. While the cells under ectodermal differentiation condition maintained a

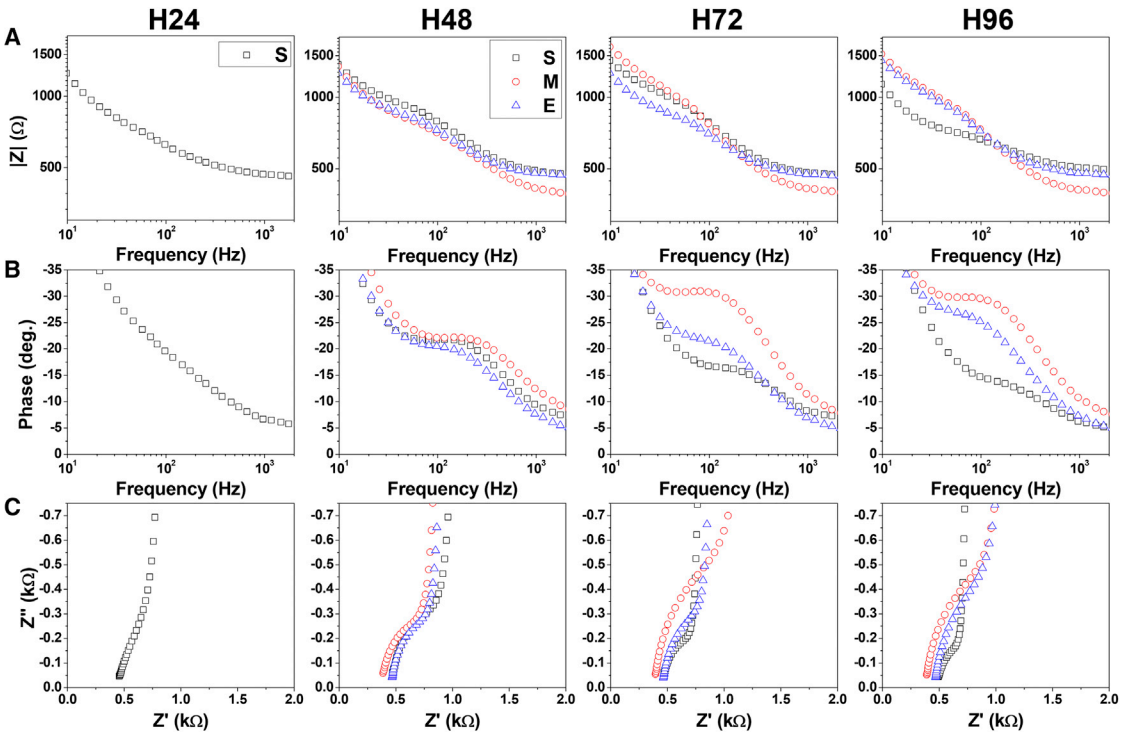

Figure 5. Impedance Measurements of IPSC Self-renewal or Differentiation by EIS

Representative (A) Bode magnitude, (B) Bode phase, and (C) Nyquist plots of EIS measurements at hours 48, 72, and 96 for IPSCs subjected to self-renewal or differentiation (S, self-renewal; M, mesendodermal differentiation; E, ectodermal differentiation). See also Figure S3.

relatively constant mass, those under self-renewal and mesendodermal differentiation conditions exhibited a decrease in mass. Combined with the optical observation where all three conditions maintained 100% confluency after hour 60, these results suggest that there are significant changes in cell number and morphology (e.g., size) among the three conditions. Pearson's correlation analysis showed statistically significant relationship between the cell number and the mass change for each condition (self-renewal: 0.588, $p < 0.05$; mesendodermal: 0.229, $p < 0.05$; ectodermal: 0.975, $p < 0.01$).

In addition to optical observations and mass change measurements, the impedance was determined every 12 hr during the culture by EIS using the multi-modal system. Impedance changes at various time points are presented in the form of Bode magnitude/phase plots (Figures 5A and 5B), or the Nyquist plot (Figure 5C). Representative impedance datasets for the time points that exhibited significant differences in mass among the three conditions, hours 48, 72, and 96, are shown (complete datasets for all time points are shown in Figure S3). In the Bode magnitude plot at hour 48, all three conditions exhibited similar impedance values at low frequencies, indicating similar cell-substrate interaction (e.g., surface coverage by the cells) (Figure 5A). However, at high frequencies, mesendodermal differentiation exhibited a different impedance behavior, suggesting changes in cell membrane (Giaever and Keese, 1993). Over the course of IPSC culture, all three conditions showed different impedance changes, indicating differential development of the electrochemical interfaces (e.g., cell morphology, cell coverage, and cell-cell and cell-substrate interactions). The phase angle plots clearly showed a differential peak development over the duration of cell culture for the three conditions, also indicating significant differences in cell-cell and cell-substrate interactions (Figure 5B). During the culture period, for example, the mesendodermal differentiation condition formed a shoulder, while self-renewal lost its shoulder approximately at 200 Hz. Similar to the Bode plots, the Nyquist spectra also showed clear differences in resistance and capacitance of the cells subjected to different conditions at various time points (Figure 5C). However, these impedance data do not readily deconvolute the contributions of cellular and extracellular components and their resistive and capacitive behaviors.

Equivalent Circuit Modeling

For a detailed analysis of impedance changes during the cell culture, an equivalent circuit model based on a

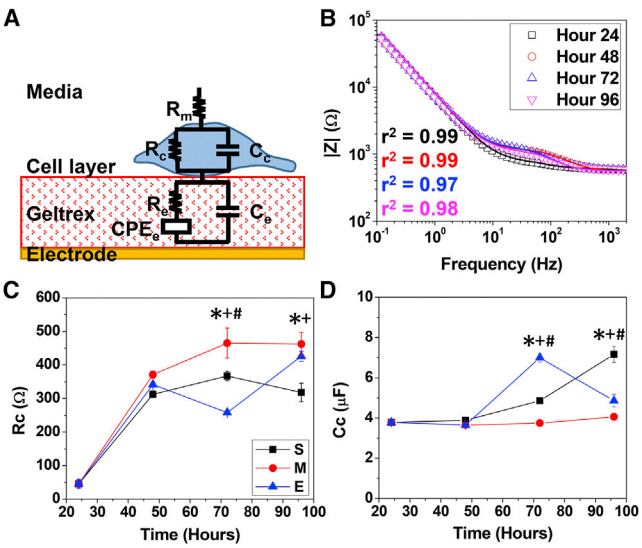

Figure 6. Equivalent Circuit Modeling of IPSCs

(A) A schematic of an equivalent circuit model for Geltrex/electrode-IPSC-culture medium interfaces consisted of resistance, capacitance, and CPE of the extracellular components (R_e, C_e, and CPE), resistance and capacitance of cellular components (R_c and C_c), and resistance of cell culture medium solution (R_m).

(B) Representative Bode magnitude curves fitted with the equivalent circuit model for self-renewal (scattered plot, experimental data; line plot, fitted data).

(C) R_c and (D) C_c values derived from the equivalent circuit model over the course of cell culture period (S, self-renewal; M, mesendodermal differentiation; E, ectodermal differentiation). Data are represented by mean ± SEM (n = 3; 3 independent experiments). $^{*,+,\#}p < 0.05$ between S and M, S and E, and M and E, respectively (see also Figure S4).

cell/protein layer/electrode system was utilized (Qiu et al., 2008). The model consists of the resistance of the medium (R_m), the impedance of the cellular components (resistance, R_c; capacitance, C_c), and the impedance of the extracellular components (Geltrex/electrode; resistance, R_e; capacitance, C_e; and constant phase element, CPE_e) (Figure 6A). Assuming that Z_c (combination of R_c and C_c) is the only component significantly changing during culture, fixed values for R_m and Z_e (R_e, C_e, and CPE_e) were determined by direct solution measurement and impedance measurement without cells, respectively. Figure 6B shows a relatively good fitting of the equivalent circuit model on the representative experimental data for the self-renewal condition (a complete set of fitted data can be found in Figure S4). The fitted values of R_c and C_c from impedance results of IPSCs during the course of self-renewal and differentiation are presented in Figures 6C and 6D, respectively. There was a steady increase in R_c in all conditions up to hour 48, after which different behaviors were observed (Figure 6C). R_c was strongly correlated to the changes of cell number as determined by Pearson's correlation analysis (self-renewal: 0.717, $p < 0.01$; mesendodermal differentiation: 0.927, $p < 0.01$; ectodermal differentiation: 0.927, $p < 0.01$). Interestingly, R_c was positively correlated to the cell size in the self-renewal renewal (−0.628, $p < 0.01$) and ectodermal differentiation (−0.714, $p < 0.01$) conditions, while it was negatively correlated to that in the mesendodermal differentiation condition (0.264, $p < 0.01$). C_c also exhibited different trends after reaching confluency (Figure 6D). The values for C_c increased for cells undergoing self-renewal and ectodermal differentiation after hour 48, while C_c for the mesendodermal cells remained relatively constant. The changes in C_c strongly correlate with changes in cell size for self-renewal (−0.604, $p < 0.01$) and ectodermal differentiation (−0.385, $p < 0.01$), while there is no correlation between the C_c and the cell size/morphology for the mesendodermal differentiation condition.

DISCUSSION

During stem cell differentiation, the cells undergo transient changes in cell shape until reaching end-phenotypes. These physico-morphological changes are important markers to determine the differentiation state of the cells (Neuhuber et al., 2004; Sullivan et al., 2010). Optical microscopy has been a choice of non-destructive analytical methods to monitor cellular behaviors. However, an optical analysis is semi-quantitative at best, and often subjective by observers. In this regard, a new quantitative analytical methodology enabling real-time observation of cellular behaviors in a non-destructive manner would advance our fundamental understanding in stem cell biology. Recently, Raman spectroscopy demonstrated its ability to assess the degree of stem cell differentiation by non-destructively detecting macromolecular compositional changes (Chan et al., 2009; Konorov et al., 2015; Schulze et al., 2010). However, such chemical changes are associated with protein expression, which typically occur at the later stages of stem cell differentiation. In this study, we demonstrated that the differentiation lineage/state-dependent morphological changes of human IPSCs were significantly correlated to the changes in mass and impedance spectra that were continuously monitored throughout the culture period, providing a quantitative means to determine stem cell development.

The changes in cell mass (or surface coverage) and cell morphology are the most apparent characteristic features associated with the self-renewal and differentiation of the stem cells. During IPSC self-renewal, the cell morphology relatively maintained a round and compact shape as cell surface coverage increased by the formation and expansion

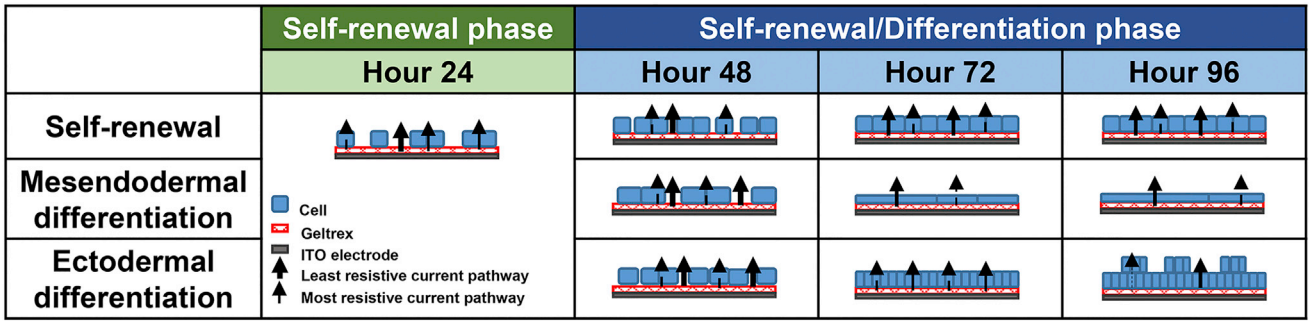

Figure 7. Proposed Mechanisms for Cellular and Electrochemical Changes during Stem Cell Self-renewal and Differentiation

of the cell colonies. In contrast, differentiation of IPSCs was marked by their transformation in cell shape as distinctive morphology was developed between differentiation toward different lineages, i.e., mesendodermal and ectodermal cells. Cells undergoing mesendodermal differentiation exhibited spreading and elongation. In contrast, cells undergoing ectodermal differentiation showed a slightly round morphology, and exhibited stacking to form a multi-layered structure at a later stage. Such overall physical changes including cell surface coverage, morphological features of individual cells, and cell-cell interactions collectively influence impedance of the cells, providing quantitative distinction among different states of cell growth/differentiation when optical visualization do not provide sufficient information.

Monitoring the mass changes provides information about general cell expansion, but it alone cannot completely depict cellular behaviors especially after reaching 100% confluency. For example, there was an increase in mass corresponding to an increase in surface coverage up 100% coverage at hour 60. Following hour 60, there were differences in mass change patterns, yet the surface coverage remained at 100%, due to changes in cell size. In this regard, impedance measurement can supplement the missing information, i.e., cell morphology, as impedance response depends on the electrical current pathway determined by cell surface coverage and cell morphology (Giaever and Keese, 1986, 1993; Keese and Giaever, 1994; Wegener et al., 2000). As expected, impedance measurements were similar at hour 48 before the cells reached 100% surface coverage at hour 60, regardless of their culture conditions. Thereafter, differential and dynamic impedance changes were observed among the conditions, likely due to the combinational effects from lineage-/stage-dependent cell morphology changes. Interestingly, after the cells undergoing ectodermal differentiation reached 100% confluency, up to which similar mass and impedance changes to the self-renewal condition were observed, there was a differential development in impedance spectrum. Typically, cells subjected to ectodermal differentiation become tightly packed to form neural rosettes (Elkabetz et al., 2008; Warren et al., 2010). These tightly packed cells stack on top of each other, therefore affecting the electrical pathway, leading to possible increase in impedance at lower frequencies. In contrast, cells undergoing mesendodermal differentiation exhibited a slightly different development of impedance spectrum from the initiation of differentiation compared with the other conditions. This is likely due to the changes in cell shape before reaching 100% confluency. The changes in cell size and morphology continued with a mass decrease while maintaining 100% surface coverage. This resulted in fewer cell-cell junctions, which may have led to the changes in impedance. However, it is not readily possible to decouple the individual contributions of such changes in cell coverage, shape, and cell-cell/cell-substrate interactions from the overall impedance of the complex system.

In this regard, equivalent circuit modeling provides a means to extract the contribution of individual components (i.e., cell, substrate, and cell culture medium) from overall impedance changes. There were several studies that attempted to characterize stem cell differentiation via monitoring impedance measurements at a specific frequency (Angstmann et al., 2011; Hildebrandt et al., 2010; Park et al., 2011). While those studies pioneered the application of EIS in the stem cell field, they were limited to comparing impedance changes with unidentified cellular changes during stem cell differentiation in a semi-quantitative manner. The studies lacked the full realization of electrochemical analysis to link physico-morphological changes associated with various stem cell states. In contrast, our study attempts to correlate the relationship between the changes in specific physical properties and electrochemical responses of IPSCs in order to characterize stem cell development. An equivalent circuit model was utilized to dissect the individual contributions from resistive and capacitive reactances of the cellular components. A mechanism model for impedance responses associated with cell morphology changes during stem cell self-renewal/differentiation is proposed in Figure 7. As shown in Figure 6, R_c, resistance of the cells, increased

proportionally with cell coverage before it reached 100% confluency at hour 60. The fastest expansion of cell colonies during this period under the self-renewal condition likely led to the greatest resistance increase compared with the differentiation conditions. At a later stage, there was a decrease in R_c in the self-renewal condition, while an increase was observed in the ectodermal differentiation condition. Considering the fact that the conditions have relatively similar cell number and morphology changes, cell stacking in the ectodermal differentiation may result in a greater resistance. For mesendodermal differentiation, after 100% confluency, cell size continued to increase, leading to fewer cell-cell junctions and the highest R_c.

Changes in C_c typically indicate alterations in the cell membrane (Benson et al., 2013; de Roos et al., 1996; Jo et al., 2015). Clear differences in C_c among the conditions began to appear after the cells reached 100% confluency. As expected, there was a strong correlation between C_c to cell size, indicating that cellular capacitance depends on the membrane area. The C_c of self-renewing cells and cells undergoing ectodermal differentiation gradually increased up to hour 72, strongly correlated with cell size decreases, and hence with increased membrane area. Differences in C_c become apparent between the two conditions at the later stage where there is a decrease in C_c in the ectodermal differentiation condition, probably due to stacking. However, the C_c for mesendodermal cells remained relatively constant unlike the other conditions. During mesendodermal differentiation, cell size increases while they elongate (decrease in circularity and increase in aspect ratio), effectively maintaining a relatively uniform cell membrane area. This probably resulted in statistically insignificant correlation between the capacitance of mesendodermal cells and their size/shape. Nevertheless, the deconvolution of electrical components demonstrated lineage and stage-specific changes, enabling the determination of stem cell behaviors during self-renewal and differentiation.

Although we have not tested this multi-modal system for different kinds of stem cells, we fully expect that any stem cell differentiation associated with mass and morphology changes can be detected by the system. This is supported by the observation that lineage-specific impedance changes at a specific frequency occur during osteogenic and adipogenic differentiation of mesenchymal stem cells (Bagnaninchi and Drummond, 2011). In addition, the system should be able to distinguish further lineage specification that induces morphological changes, e.g., cell alignment and elongation during long-term cardiac and neural differentiation, which affect cell-substrate and cell-cell interactions, and thus impedance. The EIS measurements can be continuously conducted without affecting cellular behaviors for any culture duration as long as the cells do not detach from the QCM crystal (Bagnaninchi and Drummond, 2011). However, the system cannot detect cellular behaviors that are not associated with morphological changes (i.e., protein secretion). In this regard, the use of the QCM-EIS system complemented by another non-destructive, label-free analytical tool that can detect chemical/macromolecular changes, such as Raman spectroscopy, would further enhance the analysis of cellular behaviors.

In summary, we have demonstrated that our multi-modal system offers a powerful technology to non-destructively monitor stem cell behaviors in real time by incorporating three analytical techniques, QCM, EIS, and optical microscopy. The combination of QCM and EIS provides the capability to simultaneously quantify cellular mass change and the electrical impedance of the system; QCM provides information about cell growth, while EIS offers a means to characterize cell morphology changes. In addition, the optical visualization capability allows linking such physico-electrochemical changes to the morphological changes of the cells. Therefore, the combination of this quantitative information and electrical circuit modeling collectively offers a means for an in-depth understanding of cellular processes during stem cell self-renewal and differentiation.

EXPERIMENTAL PROCEDURES

QCM Crystal Preparation

The ITO QCM crystal (MicroVacuum) was cleaned by ultrasonication in the sequence of acetone, isopropanol, then deionized water for 30 min per bath, followed by drying in a gentle flow of nitrogen gas. The crystal was subjected to 30 s of oxygen plasma treatment (Electron Microscopy Sciences) at 30 W, then sterilization with 70% ethanol for 1 hr, and subsequent UV sterilization for 30 min. A commercially available basement membrane matrix, Geltrex (Life Technologies), was coated onto the crystal surface overnight. The Geltrex layer allows for better IPSC attachment and adhesion. Following the completion of each experiment, the crystal was subjected to an ammonia-peroxide water mixture (1:1:5 volume ratio of NH_4OH, H_2O_2, and H_2O, respectively) for 5 min at 75°C to effectively remove secreted proteins adhered to the crystal surface.

IPSC Culture

A well-characterized human IPSC line was utilized in this study (Maldonado et al., 2016a, 2016b, 2015). Cells were seeded on to the Geltrex-coated QCM crystal at approximately 75,000 cells/cm^2. The cells were then cultured in an incubator for 24 hr at 37°C and 5% CO_2 with mTeSR1 maintenance medium (STEMCELL Technologies) supplemented by a ROCK inhibitor (Y-27632, 1:1000, Reagents Direct) to ensure cell survival and attachment. After the 24 hr of incubation, when the cells were at approximately 40% confluency, the cell-seeded ITO QCM crystal was then assembled into the device. The ROCK inhibitor was removed from the culture medium and cells were maintained in mTeSR1 to monitor self-renewal until

reaching 70% confluency. Cells were then cultured for 72 hr under mTeSR1 maintenance medium or subjected to mesendodermal or ectodermal differentiation. Optical images using a microscope were taken every 12 hr to monitor changes in cell morphology and quantify surface coverage. For the positive controls, the same batches of IPSCs were seeded at the same seeding density onto Geltrex-coated glass coverslips in a tissue culture plate. Samples were fixed every 12 hr with 4% paraformaldehyde (Fisher Scientific) and stored in PBS for subsequent immunocytochemistry.

In Vitro Differentiation of IPSC toward Mesendodermal and Ectodermal Lineages

Differentiation was induced at 70% cell confluency. For mesendodermal differentiation, the cells were subjected to a medium composed of DMEM-F12, L-glutamine, ITS, non-essential amino acids, B27, and β-mercaptoethanol supplemented with the following growth factors: day 1: 25 ng/μL Wnt3a (R&D Systems), 10 μg/μL Activin-A (PeproTech); day 2: 25 ng/μL Wnt3a, 10 μg/mL Activin-A, 4 ng/mL bFGF (R&D Systems); and day 3: 25 ng/μL Wnt3a, 10 μg/μL Activin-A, 4 ng/μL bFGF, 50 ng/μL BMP4 (R&D Systems) (Maldonado et al., 2016a). The medium was exchanged daily in the QCM-EIS device, as well as for the positive controls.

For ectodermal differentiation, the cells were maintained in neurobasal medium, supplemented with B27, N2, L-glutamine, and non-essential amino acids. The medium was exchanged every 36 hr with the growth factors, 0.1 μM retinoic acid (Sigma-Aldrich), and 2 μM dorsomorphin (Sigma-Aldrich), according to an established protocol for ectodermal differentiation (Maldonado et al., 2016a). The positive controls were treated on the same schedule.

Protein and Gene Expression of IPSC Self-renewal and Differentiation

Fixed cells of the positive control samples were stained for NANOG, a pluripotency marker, to confirm the maintenance of pluripotency during the culture; Goosecoid (GSC), a mesendodermal marker (R&D Systems), and Nestin, an ectodermal marker (DSHB) to confirm the presence of differentiated cells. DAPI (Vector Laboratories) and Phalloidin (Life Technologies) staining were used to identify nuclei and actin structure, respectively.

Alternatively, the maintenance of pluripotency, or differentiation toward mesendodermal or ectodermal lineage, was confirmed at the gene level by real-time PCR. Total RNA from the positive control samples was extracted using an RNeasy Micro Kit (QIAGEN), and cDNA synthesis was performed using an iScript cDNA Synthesis Kit (Bio-Rad) according to the manufacturers' protocols. Real-time PCR was performed to determine the gene expression of pluripotency and various differentiation markers using the custom primers (Table S1). Data were analyzed by the comparative threshold cycle (C_T) method using *GAPDH* as an endogenous control (Livak and Schmittgen, 2001).

Quantification of Nucleus Morphology

The shape descriptors feature from ImageJ was utilized to quantify the area, circularity, and aspect ratio of nuclei from immunofluorescent images (Rocca et al., 2015). A total of 450 cells from nine images taken from different areas of three biologically independent samples per condition were subjected to morphological characterization. Circularity is defined with $4\pi \times (Area)/(Perimeter)^2$, with a value of 1.0 indicating a perfect circle, and a value approaching 0 representing an elongated shape. The aspect ratio is calculated by a/b, where a and b are defined as the primary and secondary axis, respectively, of the best fitting ellipse.

Mass Change and Impedance Measurements during Cell Culture

The QCM function of the system continuously monitored changes in cell mass throughout the cell culture period. EIS was set to measure impedance by applying an AC perturbation of 10 mV using a potentiostat (CH Instruments) every 12 hr. The frequency sweep ranged between 10^{-1} to 10^4 Hz with 12 measurements performed per decade. The resulting data provided impedance values (real, imaginary, and magnitude), and phase shift that corresponded to each frequency measurement.

Fitting and Simulation

EIS Analyser software was used to fit the experimental data with the proposed equivalent circuit model. The circuit model was modified from the previous study of Qiu et al. (2008). The Nelder-Mead algorithm was utilized to determine the fixed circuit values for the impedance of the extracellular components without cells. Once the fixed values were determined, the same algorithm was used to determine the impedance of the cellular components.

Statistics

QCM and EIS measurements were repeated in triplicate with different batches of human IPSCs. The same batch of cells was used for the positive controls with at least three samples per condition for morphological characterization. Data are presented as means ± SEM. Student's t test was used to determine statistical significance of gene expression. Pearson's correlation coefficient was determined to reveal bivariate correlation between cellular characteristics (number, size, and shape) and measured impedance (resistance and capacitance). Statistical significance among the experimental conditions (i.e., self-renewal to mesendodermal differentiation, self-renewal to ectodermal differentiation, and mesendodermal differentiation to ectodermal differentiation) for cell number, morphological features, the resistive and capacitive values from EIS measurements/model fitting were determined by ANOVA with Tukey's post-hoc test. It was considered statistically significant when a p value was less than 0.05.

SUPPLEMENTAL INFORMATION

Supplemental Information includes four figures and one table and can be found with this article online at http://dx.doi.org/10.1016/j.stemcr.2017.03.021.

AUTHOR CONTRIBUTIONS

Device Design and Development, K.L., L.W., C.M., C.B.H., M.P., N.V.M., and J.N.; Data Collection, K.L., L.W., M.M.; Data Analysis

and Interpretation, K.L., L.W., N.V.M., and J.N.; Manuscript Writing, K.L., L.W., N.V.M., and J.N.

ACKNOWLEDGMENTS

This study was supported by the UCR Initial Complement Fund and the UCR Stem Cell Core Facility, funded by CIRM.

Received: December 20, 2016
Revised: March 27, 2017
Accepted: March 28, 2017
Published: April 27, 2017

REFERENCES

Amabile, G., and Meissner, A. (2009). Induced pluripotent stem cells: current progress and potential for regenerative medicine. Trends Mol. Med. *15*, 59–68.

Angstmann, M., Brinkmann, I., Bieback, K., Breitkreutz, D., and Maercker, C. (2011). Monitoring human mesenchymal stromal cell differentiation by electrochemical impedance sensing. Cytotherapy *13*, 1074–1089.

Bagnaninchi, P.O., and Drummond, N. (2011). Real-time label-free monitoring of adipose-derived stem cell differentiation with electric cell-substrate impedance sensing. Proc. Natl. Acad. Sci. USA *108*, 6462–6467.

Benson, K., Cramer, S., and Galla, H.-J. (2013). Impedance-based cell monitoring: barrier properties and beyond. Fluids Barriers CNS *10*, 5.

Burkhardt, M.F., Martinez, F.J., Wright, S., Ramos, C., Volfson, D., Mason, M., Garnes, J., Dang, V., Lievers, J., and Shoukat-Mumtaz, U. (2013). A cellular model for sporadic ALS using patient-derived induced pluripotent stem cells. Mol. Cell Neurosci. *56*, 355–364.

Chan, J.W., Lieu, D.K., Huser, T., and Li, R.A. (2009). Label-free separation of human embryonic stem cells and their cardiac derivatives using Raman spectroscopy. Anal. Chem. *81*, 1324–1331.

Chen, C., Jiang, P., Xue, H., Peterson, S.E., Tran, H.T., McCann, A.E., Parast, M.M., Li, S., Pleasure, D.E., Laurent, L.C., et al. (2014a). Role of astroglia in Down's syndrome revealed by patient-derived human-induced pluripotent stem cells. Nat. Commun. *5*, 4430.

Chen, H., Qian, K., Du, Z., Cao, J., Petersen, A., Liu, H., Blackbourn, L.W., Huang, C.-L., Errigo, A., and Yin, Y. (2014b). Modeling ALS with iPSCs reveals that mutant SOD1 misregulates neurofilament balance in motor neurons. Cell Stem Cell *14*, 796–809.

Cyranoski, D. (2014). Japanese woman is first recipient of next-generation stem cells. Nature http://dx.doi.org/10.1038/nature.2014.15915.

de Roos, A.D., van Zoelen, E.J., and Theuvenet, A.P. (1996). Determination of gap junctional intercellular communication by capacitance measurements. Pflügers Arch. *431*, 556–563.

Ebert, A.D., Liang, P., and Wu, J.C. (2012). Induced pluripotent stem cells as a disease modeling and drug screening platform. J. Cardiovasc. Pharmacol. *60*, 408–416.

Egawa, N., Kitaoka, S., Tsukita, K., Naitoh, M., Takahashi, K., Yamamoto, T., Adachi, F., Kondo, T., Okita, K., and Asaka, I. (2012). Drug screening for ALS using patient-specific induced pluripotent stem cells. Sci. Transl. Med. *4*, 145ra104.

Elkabetz, Y., Panagiotakos, G., Al Shamy, G., Socci, N.D., Tabar, V., and Studer, L. (2008). Human ES cell-derived neural rosettes reveal a functionally distinct early neural stem cell stage. Genes Dev. *22*, 152–165.

Giaever, I., and Keese, C.R. (1986). Use of electric fields to monitor the dynamical aspect of cell behavior in tissue culture. IEEE Trans. Biomed. Eng. *33*, 242–247.

Giaever, I., and Keese, C.R. (1993). A morphological biosensor for mammalian cells. Nature *366*, 591.

Hildebrandt, C., Büth, H., Cho, S., and Thielecke, H. (2010). Detection of the osteogenic differentiation of mesenchymal stem cells in 2D and 3D cultures by electrochemical impedance spectroscopy. J. Biotechnol. *148*, 83–90.

Hu, B.Y., Weick, J.P., Yu, J., Ma, L.X., Zhang, X.Q., Thomson, J.A., and Zhang, S.C. (2010). Neural differentiation of human induced pluripotent stem cells follows developmental principles but with variable potency. Proc. Natl. Acad. Sci. USA *107*, 4335–4340.

Jo, D.H., Lee, R., Kim, J.H., Jun, H.O., Lee, T.G., and Kim, J.H. (2015). Real-time estimation of paracellular permeability of cerebral endothelial cells by capacitance sensor array. Sci. Rep. *5*, 11014.

Keese, C.R., and Giaever, I. (1994). A biosensor that monitors cell morphology with electrical fields. IEEE Eng. Med. Biol. Mag. *13*, 402–408.

Kim, C. (2014). Disease modeling and cell based therapy with iPSC: future therapeutic option with fast and safe application. Blood Res. *49*, 7–14.

Konorov, S.O., Schulze, H.G., Gage, B.K., Kieffer, T.J., Piret, J.M., Blades, M.W., and Turner, R.F.B. (2015). Process analytical utility of Raman microspectroscopy in the directed differentiation of human pancreatic insulin-positive cells. Anal. Chem. *87*, 10762–10769.

Livak, K.J., and Schmittgen, T.D. (2001). Analysis of relative gene expression data using real-time quantitative PCR and the $2^{-\Delta\Delta CT}$ method. Methods *25*, 402–408.

Maldonado, M., Wong, L.Y., Echeverria, C., Ico, G., Low, K., Fujimoto, T., Johnson, J.K., and Nam, J. (2015). The effects of electrospun substrate-mediated cell colony morphology on the self-renewal of human induced pluripotent stem cells. Biomaterials *50*, 10–19.

Maldonado, M., Ico, G., Low, K., Luu, R.J., and Nam, J. (2016a). Enhanced lineage-specific differentiation efficiency of human induced pluripotent stem cells by engineering colony dimensionality using electrospun scaffolds. Adv. Healthc. Mater. *5*, 1408–1412.

Maldonado, M., Luu, R.J., Ramos, M.E.P., and Nam, J. (2016b). ROCK inhibitor primes human induced pluripotent stem cells to selectively differentiate towards mesendodermal lineage via epithelial-mesenchymal transition-like modulation. Stem Cell Res. *17*, 222–227.

Meissner, A., Wernig, M., and Jaenisch, R. (2007). Direct reprogramming of genetically unmodified fibroblasts into pluripotent stem cells. Nat. Biotechnol. *25*, 1177–1181.

Morgan, H., Sun, T., Holmes, D., Gawad, S., and Green, N.G. (2007). Single cell dielectric spectroscopy. J. Phys. D Appl. Phys. *40*, 61–70.

Neuhuber, B., Gallo, G., Howard, L., Kostura, L., Mackay, A., and Fischer, I. (2004). Reevaluation of in vitro differentiation protocols for bone marrow stromal cells: disruption of actin cytoskeleton induces rapid morphological changes and mimics neuronal phenotype. J. Neurosci. Res. *77*, 192–204.

Oldershaw, R.A., Baxter, M.A., Lowe, E.T., Bates, N., Grady, L.M., Soncin, F., Brison, D.R., Hardingham, T.E., and Kimber, S.J. (2010). Directed differentiation of human embryonic stem cells toward chondrocytes. Nat. Biotechnol. *28*, 1187–1194.

Park, H.E., Kim, D., Koh, H.S., Cho, S., Sung, J.-S., and Kim, J.Y. (2011). Real-time monitoring of neural differentiation of human mesenchymal stem cells by electric cell-substrate impedance sensing. J. Biomed. Biotechnol. *2011*, 485173.

Qiao, G., Wang, W., Duan, W., Zheng, F., Sinclair, A.J., and Chatwin, C.R. (2012). Bioimpedance analysis for the characterization of breast cancer cells in suspension. IEEE Trans. Biomed. Eng. *59*, 2321–2329.

Qiu, Y., Liao, R., and Zhang, X. (2008). Real-time monitoring primary cardiomyocyte adhesion based on electrochemical impedance spectroscopy and electrical cell-substrate impedance sensing. Anal. Chem. *80*, 990–996.

Randviir, E.P., and Banks, C.E. (2013). Electrochemical impedance spectroscopy: an overview of bioanalytical applications. Anal. Methods *5*, 1098–1115.

Rocca, A., Marino, A., Rocca, V., Moscato, S., de Vito, G., Piazza, V., Mazzolai, B., Mattoli, V., Ngo-Anh, T.J., and Ciofani, G. (2015). Barium titanate nanoparticles and hypergravity stimulation improve differentiation of mesenchymal stem cells into osteoblasts. Int. J. Nanomedicine *10*, 433–445.

Schulze, H.G., Konorov, S.O., Caron, N.J., Piret, J.M., Blades, M.W., and Turner, R.F.B. (2010). Assessing differentiation status of human embryonic stem cells noninvasively using Raman microspectroscopy. Anal. Chem. *82*, 5020–5027.

Sullivan, G.J., Hay, D.C., Park, I.-H., Fletcher, J., Hannoun, Z., Payne, C.M., Dalgetty, D., Black, J.R., Ross, J.A., Samuel, K., et al. (2010). Generation of functional human hepatic endoderm from human induced pluripotent stem cells. Hepatology *51*, 329–335.

Venkatanarayanan, A., Keyes, T.E., and Forster, R.J. (2013). Label-free impedance detection of cancer cells. Anal. Chem. *85*, 2216–2222.

Versaevel, M., Grevesse, T., and Gabriele, S. (2012). Spatial coordination between cell and nuclear shape within micropatterned endothelial cells. Nat. Commun. *3*, 671.

Vishavkarma, R., Raghavan, S., Kuyyamudi, C., Majumder, A., Dhawan, J., and Pullarkat, P.A. (2014). Role of actin filaments in correlating nuclear shape and cell spreading. PLoS One *9*, e107895.

Wang, S., Wang, B., Pan, N., Fu, L., Wang, C., Song, G., An, J., Liu, Z., Zhu, W., Guan, Y., et al. (2015). Differentiation of human induced pluripotent stem cells to mature functional Purkinje neurons. Sci. Rep. *5*, 9232.

Warren, L., Manos, P.D., Ahfeldt, T., Loh, Y.-H., Li, H., Lau, F., Ebina, W., Mandal, P.K., Smith, Z.D., Meissner, A., et al. (2010). Highly efficient reprogramming to pluripotency and directed differentiation of human cells with synthetic modified mRNA. Cell Stem Cell *7*, 618–630.

Wegener, J., Keese, C.R., and Giaever, I. (2000). Electric cell-substrate impedance sensing (ECIS) as a noninvasive means to monitor the kinetics of cell spreading to artificial surfaces. Exp. Cell Res. *259*, 158–166.

Yu, J., Vodyanik, M.A., Smuga-Otto, K., Antosiewicz-Bourget, J., Frane, J.L., Tian, S., Nie, J., Jonsdottir, G.A., Ruotti, V., and Stewart, R. (2007). Induced pluripotent stem cell lines derived from human somatic cells. Science *318*, 1917–1920.